ACS APPLIED MATERIALS & INTERFACES

Research Article

Cite This: ACS Appl. Mater. Interfaces 2018, 10, 27850−27857

www.acsami.org

Silicon/Perovskite Core−Shell Heterojunctions with Light-Trapping Effect for Sensitive Self-Driven Near-Infrared Photodetectors

Jia-Qin Liu,[†] Yang Gao,[†] Guo-An Wu,[‡] Xiao-Wei Tong,[‡] Chao Xie,*[,‡] Lin-Bao Luo,*[,‡] Lin Liang,[§] and Yu-Cheng Wu*[,§]

[†]Institute of Industry & Equipment Technology and Anhui Provincial Key Laboratory of Advanced Functional Materials and Devices, Hefei University of Technology, Hefei 230009, China

[‡]School of Electronic Science & Applied Physics and [§]School of Materials Science & Engineering, Hefei University of Technology, Hefei, Anhui 230009, China

Supporting Information

ABSTRACT: In this article, we fabricated a sensitive near-infrared (NIR) light detector by directly coating a layer of Cs-doped $FAPbI_3$ perovskite film onto vertical Si nanowire (SiNW) array. The as-assembled SiNW array/perovskite core−shell heterojunction exhibits a typical rectifying characteristic in darkness and distinct photoresponse characteristics under light illumination. Owning to the remarkable photovoltaic effect, the heterojunction can work as a self-driven NIR detector without an exterior energy supply. Further photoresponse investigation reveals that the photodetector is sensitive in a wide wavelength range with maximum sensitivity at ∼850 nm. The responsivity (R) and specific detectivity (D^*) are estimated to be 14.86 mA W^{-1} and 2.04 × 10^{10} Jones at 0 V bias, respectively, which can be improved to 844.33 mA W^{-1} and 3.2 × 10^{11} Jones at a bias voltage of −0.9 V. In addition, the present device also possesses distinct advantages of a large I_{light}/I_{dark} ratio exceeding 10^4, swift response rate with rise/decay times of 4/8 μs, and relatively good ambient stability. According to our numerical simulation based on finite element method, the superior device performance is associated with strong light-trapping effect in such unique core−shell heterojunction array.

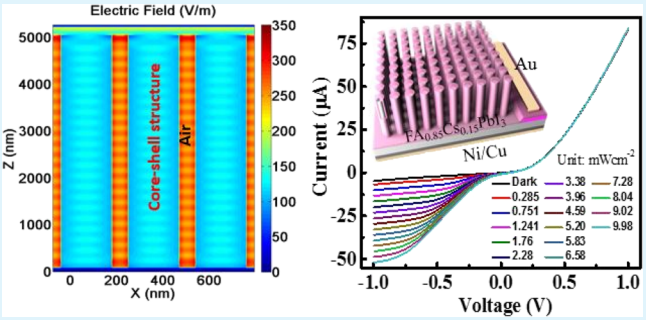

KEYWORDS: *silicon nanowires array, perovskite, heterojunction, self-driven, photodetector*

INTRODUCTION

High-performance infrared photodetectors have demonstrated wide applications in various areas such as missile guidance, military surveillance, night vision, medical diagnostics, remote temperature sensing, and so on.[1−3] The current near-infrared (NIR) light detection market is mainly dominated by the products based on bulk-crystalline Si, whose response wavelength is below 1100 nm, and the devices made from Ge/Si hybrid heterostructure or III−V semiconductor compounds (e.g., InGaAs and related heterojunction) which usually operate at a wavelength spectrum beyond 1100 nm.[4,5] Being CMOS-compatible and holding mature processing technologies, a variety of Si photodetectors with different device geometries, including p−n (or p−i−n) photodiodes, Schottky junction photodiodes, and metal−semiconductor−metal (M−S−M) detectors have been realized to date.[6] Among these photonic devices, p−n (or p−i−n) and Schottky junction diodes that are characterized by strong built-in electric field facilitating fast separation and transport of photocarriers[7] have attracted considerable attention for the low energy consumption and high-frequency optical-sensing applications. However, the assembly of Si p−n (or p−i−n) junctions typically requires high-temperature ion diffusion or costly implantation processes,[8] whereas light shadowing or metal ion diffusion issues usually exist in the Si Schottky junctions.[9] Inevitably, the complex fabrication processes and the expensive equipment, as well as the obvious drawbacks, lead to high cost of the photodetectors and deterioration in device performance. In contrast, heterojunction photodetectors composed of Si and other emerging semiconductors usually hold remarkable features such as ease of processing, low cost, complementary material properties, as well as good device performance, and have thus been of particular interest.[10−13]

Compared with the bulk and thin-film counterparts, vertical Si nanowire (SiNW) array affords great advantages for optoelectronic applications because this structure provides combined merits of suppressed light reflection, increased interfacial area, and prolonged photocarrier lifetime originating from large surface-to-volume ratio and shortened carrier transit time.[14,15] By this token, SiNW array has been regarded as an

Received: May 21, 2018
Accepted: July 30, 2018
Published: July 30, 2018

DOI: 10.1021/acsami.8b08387
ACS Appl. Mater. Interfaces 2018, 10, 27850−27857

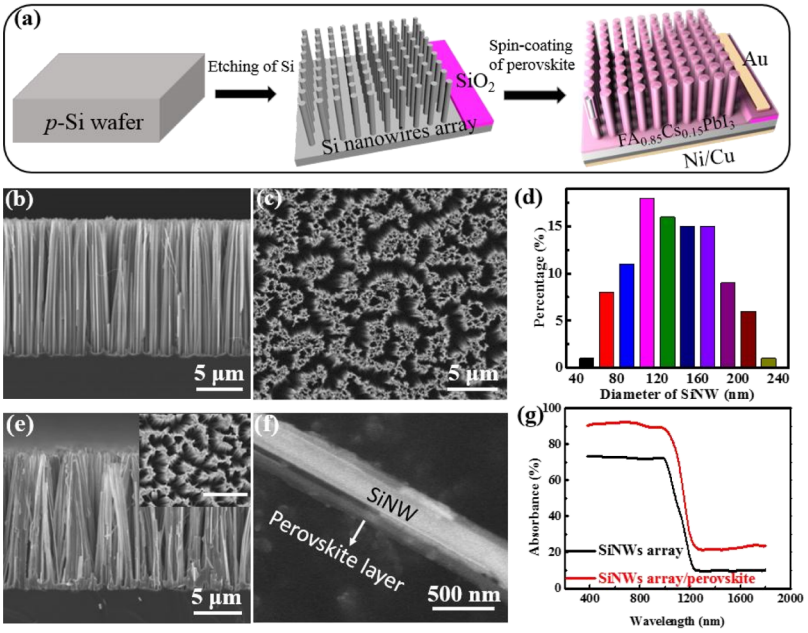

Figure 1. (a) Processes schematic for assembly of the SiNW array/perovskite heterojunction photodetector. (b) Cross-sectional and (c) top-view SEM images of the SiNW array. (d) Numerical distribution of the diameter of the as-etched NWs. (e) SEM image of the SiNW array coated with perovskite film; the inset corresponds to the top-view SEM image with scale bar of 10 μm. (f) Magnified SEM image of the single SiNW coated with perovskite, indicating formation of a typical core−shell geometry. (g) Absorption of the SiNW array/Cs-doped $FAPbI_3$ heterostructure and pure SiNW array.

ideal building block for assembly of high-performance photodetectors.[16−20] For example, by simply drop-casting the graphene oxide onto the surface of free-standing SiNW array, followed by heat-treatment, a broadband photodetector based on SiNW array/reduced GO heterojunction has been reported.[21] Such a heterojunction is sensitive to infrared, visible, and even terahertz wave radiations. Our group has also developed a photovoltaic-type detector, which was composed of carbon quantum dots (QDs) coated on vertical SiNW array.[22] The as-assembled core−shell heterojunction photodetector has achieved a high responsivity of 353 mA W^{-1} at a bias of 0 V and is capable of following rapid optical signals with a fast response speed of 20 μs.

Inspired by the above achievements, we herein report a sensitive NIR photodetector by coating a vertical SiNW array with a layer of Cs-doped $FAPbI_3$ film, which displays good air stability than undoped $FAPbI_3$. The good stability, along with the intriguing optical and electrical characteristics (e.g., suitable band gap, wideband light absorption, etc.), makes Cs-doped $FAPbI_3$ an ideal material for various optoelectronic devices application.[23−26] It is observed that the as-fabricated heterojunction shows an apparent rectifying characteristic in darkness, and a strong photovoltaic behavior when shined by light illumination enables the device to sense illumination without an external energy supply. Our further optoelectronic characterization finds that the heterojunction displays good sensitivity to 850 nm NIR light with the maximum I_{light}/I_{dark} ratio of 1.23×10^4, responsivity of 14.86 mA W^{-1}, and specific detectivity of 2.04×10^{10} Jones, respectively, at 0 V bias. By applying an operation bias of −0.9 V, both parameters could be improved to 844.33 mA W^{-1} and 3.20×10^{11} Jones, respectively. Furthermore, the heterojunction photodetector displays a rapid rise/decay time of 4/8 μs, allowing the device to track rapidly varying photonic signal with a high frequency of 50 kHz. The observed good performance could be ascribed to the excellent optical property, namely the strong light-trapping effect, in the core−shell heterojunction geometry, according to further theoretical calculation. In addition, the photoresponse properties are almost invariant after 3 weeks storage at air condition, suggesting good ambient stability. The relatively good device performance, together with the simple fabrication process, renders this heterojunction photodetector potentially useful for future high-performance NIR photodetection.

EXPERIMENTAL SECTION

Materials Synthesis and Characterization. The vertically aligned SiNW array was prepared by a silver-assisted HF etching method. In brief, a 1 × 1 cm^2 p-type silicon wafer (1−10 Ω cm^{-1}) with a 300 nm SiO_2 insulating layer was used. The SiO_2/Si substrate surface was first protected by spin-coating paraffin film to form an opening window of 5 × 5 mm^2, followed by HF etching to remove SiO_2. Afterward, the substrate was put into a mixed solution composed of 4.6 M HF and 0.005 M silver nitrate for 1 min, during which a thin layer of Ag nanoparticles was coated. Then, the substrate was immediately immersed into an etchant containing 4.6 M HF and 0.44 M H_2O_2. Afterward, chloroform was used to etch the paraffin protective layer. Finally, the sample was dipped sequentially into an aqueous HNO_3 and HF solution to remove silver and surface oxide, respectively, followed by washing with distilled water and drying under nitrogen stream. The precursor for synthesizing perovskite material was produced by dissolving 0.461 g of lead iodide (AR, 99%), 0.145 g of FAI (AR, 99.5%), and 0.0389 g of CsI (AR, 99.9%) in a solution containing dimethyl sulfoxide (>99.9%) and *N*,*N*-dimethylformamide (AR, 99.8%) with a volume of 200 and 800 μL, respectively. The as-mixed solution was treated with ultrasonic for 30 min to facilitate the dissolution of the chemicals. The resultant precursor was then spin-coated onto a clean glass at 1000 round per minute (rpm) for 30 s and annealed at 300 K for 15 min to form Cs-doped $FAPbI_3$ perovskite film.

The SiNW array was characterized by a field-emission scanning electron microscopy (SEM, SIRION 200 FEG). The chemical composition was studied using an energy-dispersive X-ray spectros-

DOI: 10.1021/acsami.8b08387
ACS Appl. Mater. Interfaces 2018, 10, 27850−27857

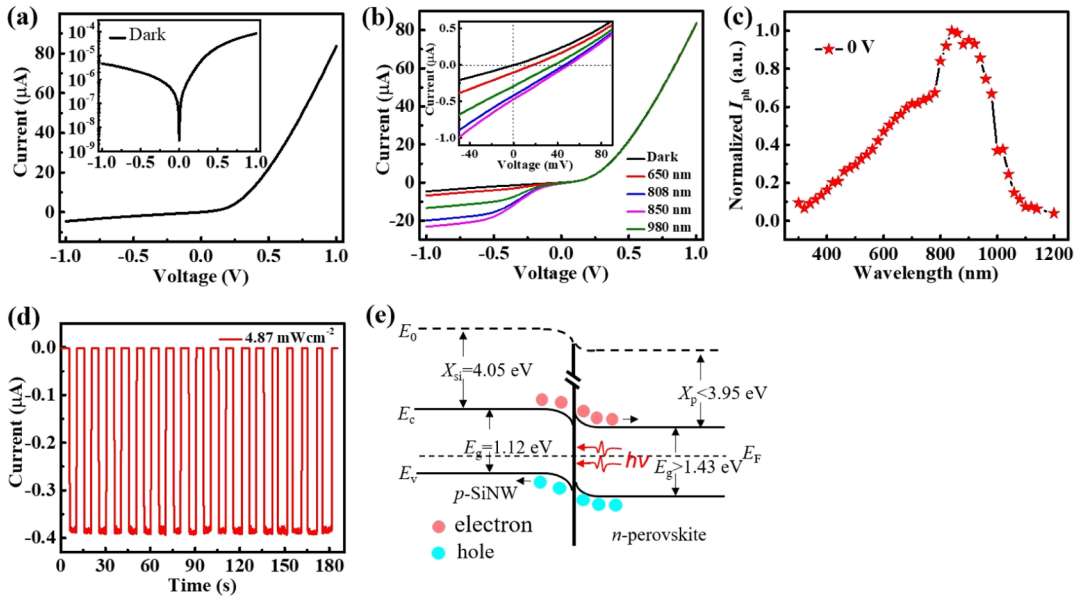

Figure 2. (a) $I-V$ curves of the SiNW array/Cs-doped $FAPbI_3$ heterojunction in darkness. (b) $I-V$ curves of the photodiode in darkness and under NIR irradiation of varied wavelengths. (c) Dependence of normalized photocurrent with the different wavelengths. (d) Time-dependent response of the photodiode under 850 nm NIR light at zero bias. (e) Energy band diagram under NIR light irradiation at 0 V.

copy (Oxford INCA). X-ray diffraction (XRD) analysis was carried out by an X-ray diffractometer (Rigaku D/max-rB) to study the microstructure of the perovskite layer. The absorption spectra of the SiNW array/perovskite heterostructure and pure SiNW array were collected by a UV−vis spectrometer (PerkinElmer/Lambda 750), which is equipped with an integrating sphere.

Device Fabrication, Analysis, and Simulation. To assemble the SiNW array/perovskite heterostructure photodiode, the above precursor was directly spin-coated onto the substrate with a window area of SiNW array. The thickness of the perovskite layer was controlled by changing the spin-coating speed, and speeds of 1000, 1500, and 2000 rpm were used in this work. Afterward, Au (50 nm) and Ni/Cu (20/30 nm) electrodes were deposited on the perovskite surface and the rear side of the wafer, respectively, via electron-beam evaporation. The device analysis was carried out using a semiconductor $I-V$ analysis instrument (Keithley Company, 4200-SCS). Laser diodes (Thorlabs L650P007, LD808-SA60, L850P010, and L980P200) with wavelengths of 650, 808, 850, and 980 nm were employed as light sources. The spectral selectivity was characterized by using a lab-built setup with a xenon lamp (5 mW cm^{-2}) and a monochromator (Omni-λ300). The response speed was investigated by a laser diode which is controlled by a signal generator (RIGOL and DG5252) to produce pulsed signal and an oscilloscope (GWINSTEK and GDS-1102A-U) to collect the signal data. The incident intensity was calibrated prior to testing.

The theoretical calculation was performed using a lab-made program based on the finite element method (FEM). Considering the periodic structure, the computational domain only comprises a single unit cell. The plane wave was used to model the incident light (850 nm) on top of the structures. Periodic boundary conditions were applied in both x and y direction to replicate the present periodic geometry. The air is semi-infinite from near to the reality. What is more, the air permittivity for this study is 1. The optical constants of Si were obtained from the Sopra S. A. Company.

RESULTS AND DISCUSSION

The Si/perovskite core−shell nanoheterojunction NIR photodiode was assembled by directly depositing a Cs-doped $FAPbI_3$ layer with higher electron mobility and better air stability onto the surface of a vertical SiNW array, which was obtained by a simple Ag-assisted HF etching approach (Figure 1a).[27,28] Figure 1b−d shows a number of SEM images of as-prepared SiNW array, as well as the corresponding statistical distribution of the NW diameter, from which one can conclude that the average length and diameter are ∼15 μm and ∼140 nm, respectively. Further SEM image in Figure 1e reveals that the surface of the SiNW becomes much rougher after coating with the perovskite film. By comparing the top-view SEM images of SiNW array without and with perovskite (Figure 1c and inset in 1e), we find that the perovskite film is prone to coating on the surface of NWs rather than filling the space between NWs. To confirm the geometry of the heterostructure, high-resolution SEM image of individual nanostructure and the corresponding elemental mapping images were recorded (Figures 1f and S1). It is revealed that the SiNW is completely encapsulated by perovskite layer, forming a typical core−shell geometry with the perovskite shell thickness of 40−50 nm (the film thickness at different speeds is shown in Figure S2). As displayed in Figure S3, XRD pattern of Cs-doped $FAPbI_3$ prepared on the glass wafer was characterized by a series of representative peaks, which is due to black-phase $FAPbI_3$.[29] Figure 1g plots the absorbance curves of both SiNW array and the SiNW array/perovskite heterostructure (the absorbance is derived by the equation $A = 1 - T - R$, where A, T, and R denote absorbance, transmittance, and reflection, respectively. The transmittance and reflection of both sample are shown in Figure S4). Clearly, both structures show broad optical absorption in the region from 400 to 1700 nm. The optimization of absorption spectrum after coating is mainly because of the guided-mode-induced enhancement. In addition, the scattering of light can contribute to the enhancement as well.[30]

Figure 2a depicts the $I-V$ characteristic of a representative SiNW/Cs-doped $FAPbI_3$ heterostructures measured in darkness. Apparently, the heterojunction exhibits current-rectifying characteristics with the ratio of ∼20 at ±1 V. Such a relatively low value can be attributed to the higher leakage current likely caused by the large amount of defects that normally exist in the spin-coated perovskite film.[31] Because Ni and Au can form

DOI: 10.1021/acsami.8b08387
ACS Appl. Mater. Interfaces 2018, 10, 27850−27857

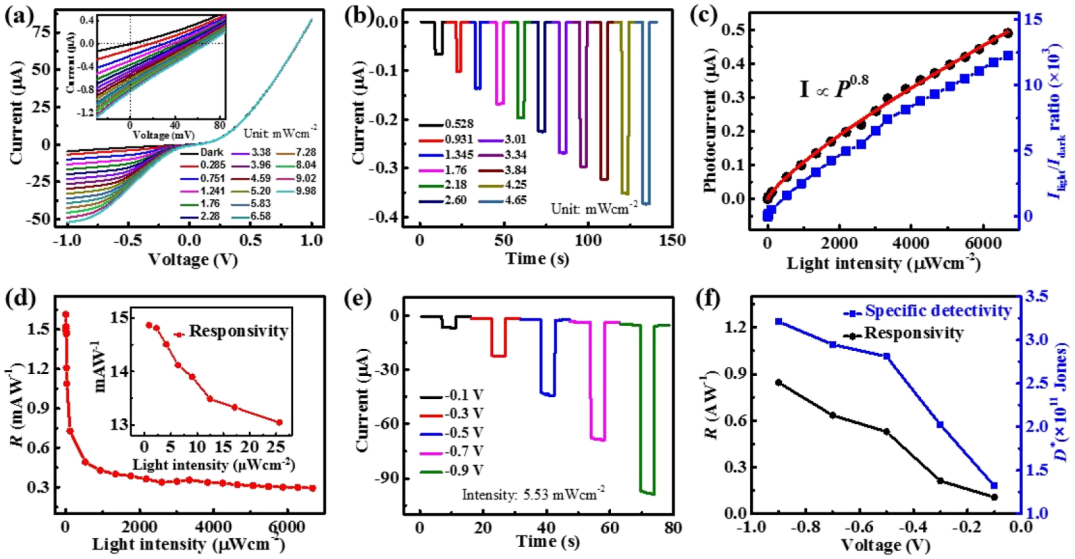

Figure 3. (a) Photoresponse curve and (b) time-dependent photoresponse of the heterojunction device under 850 nm NIR radiation of varied light intensities at near bias. (c) Photocurrent and I_{light}/I_{dark} ratio and (d) responsivity of the device under different intensities at 0 V; the inset plots the responsivity at relatively low NIR intensity. (e) Time-dependent response of the photodiode at different reverse biases. (f) Dependence of R and D^* of the device with reverse bias voltages; the light intensity is 0.892 $\mu W/cm^2$.

good Ohmic contacts with p-Si and perovskite film, respectively (Figure S5), the observed nonlinear $I-V$ behavior should arise from the heterojunction barrier of SiNW/perovskite contact. Figure 2b compares the $I-V$ characteristics of the photodiode in darkness and under irradiation with wavelengths of 650, 808, 850, and 980 nm, respectively, at a constant light intensity (3.96 mW cm^{-2}). It is found that the device is sensitive to all illuminations at reverse biases. The current first increases with the increase of wavelength from 650 to 850 nm and then reduces at relatively longer wavelength, revealing good selectivity to incident light wavelength. Careful study of the enlarged curves (inset in Figure 2b) finds weak photovoltaic behavior upon all illuminations. The strongest photovoltaic behavior is found at the wavelength of 850 nm, with an open-circuit voltage (V_{OC}) and short-circuit current (I_{SC}) of ~51 mV and ~370 nA, respectively. Although the energy-conversion efficiency is relatively low (<1%), the present device is capable of operating as a zero-powered photodiode without bias voltage. To unveil the wavelength-dependent photosensitivity, we further recorded the photocurrent at zero bias as a function of light wavelength. As observed in Figure 2c, the device exhibits a broadband photoresponse in the wavelength region of 300−1200 nm. Besides, the photodetector has a good spectral selectivity as well, with a relatively sharp response peak located at ~850 nm. The variation of photoresponse with wavelength is also in accordance with the results shown in Figure 2b. Further photoresponse analysis under switchable 850 nm NIR light reveals that the heterojunction photodiode could be easily switched on and off with a large I_{light}/I_{dark} ratio approaching 10^4 at a bias voltage of 0 V (Figure 2d). The rise and fall edges are very steep, which suggests a good photoresponse rate and also implies that photogenerated electron−hole pairs can be rapidly separated and collected in the heterojunction.

The above rectifying characteristics and photoresponse behavior is understandable from the energy band illustration shown in Figure 2e. According to Hall effect study, Cs-doped $FAPbI_3$ is a weak n-type semiconducting material with conduction band (E_C) and valence band (E_V) values of >−3.95 and <−5.38 eV, respectively.[28] Once perovskite is in contact with p-SiNW array, electrons will move from Cs-doped $FAPbI_3$ to the SiNWs until their Fermi levels are aligned at the same level. As a result, the energy levels at SiNW surface and perovskite will bend downward and upward, respectively, forming a depletion region (built-in electric field) at the SiNW/Cs-doped $FAPbI_3$ interface. Owing to this reason, the SiNW/perovskite interface will only allow current to conduct in one direction, which accounts for the observed current rectifying behavior. Similar to many heterojunction photodetectors,[8,12] when illuminated by photons with sufficient energy, electron−hole pairs will be generated in both SiNWs and perovskite. The carriers in the vicinity of the depletion region will drift to the SiNW/perovskite interface and then be separated in the depletion region. Consequently, electrons and holes will transport through perovskite film and SiNWs and are then collected by both electrodes, eventually giving rise to the formation of photocurrent.

The photoresponse of our heterojunction photodetector depends strongly on NIR intensity. Figure 3a plots the current−voltage characteristics of the photodiode under 850 nm illumination of different intensities, from which one can find that at both reverse and zero biases, the current rises with the increase of light intensity by degrees. Specifically, with the light intensity rising from 0.528 to 4.65 mW cm^{-2}, the photocurrent increases from ~65 to ~370 nA, whereas the dark current keeps almost invariant at zero bias (Figure 3b). The net photocurrent is extracted by deducing the photocurrent by dark current. As plotted in Figure 3c, the photocurrent increases monotonously with the increase of light intensity. The relationship could be described by an extensively used formula $I_{ph} = aP^b$, in which a is the parameter for incident light, P is the power of the light, and the exponent b is a constant that is related to photoresponse to light intensity, respectively. Fitting the curve gives a b = 0.8, which, however, deviates somewhat from the ideal value (b = 1). According to previous reports, such a deviation suggests that

DOI: 10.1021/acsami.8b08387
ACS Appl. Mater. Interfaces 2018, 10, 27850−27857

Table 1. Comparison of Photoresponse Parameters of Our Photodiode with Other Reported Devices with Similar Device Structures

device structure	R (A W^{-1})	I_{light}/I_{dark} ratio	D^* (Jones)	τ_r/τ_f (μs)	refs
SiNW array/perovskite	0.844	1.2×10^4	3.2×10^{11}	4/8	this work
SiNW array/CuO	0.64×10^{-4}	$\sim 10^4$	7.6×10^8	60/80	19
SiNW array/rGO	1.65×10^{-3}			10.6/6.7 s	21
SiNW array/carbon QDs	0.353	3×10^3		10/40	22
TiO_2 nanorods/perovskite	0.85	1.5×10^2	7.8×10^{10}		33
ZnO nanorods/perovskite	8.3×10^{-3}	$\sim 10^5$	$\sim 1.5 \times 10^{10}$	53/63	34
ZnO nanorods/perovskite	0.22		9.3×10^9	0.3/0.8 s	35

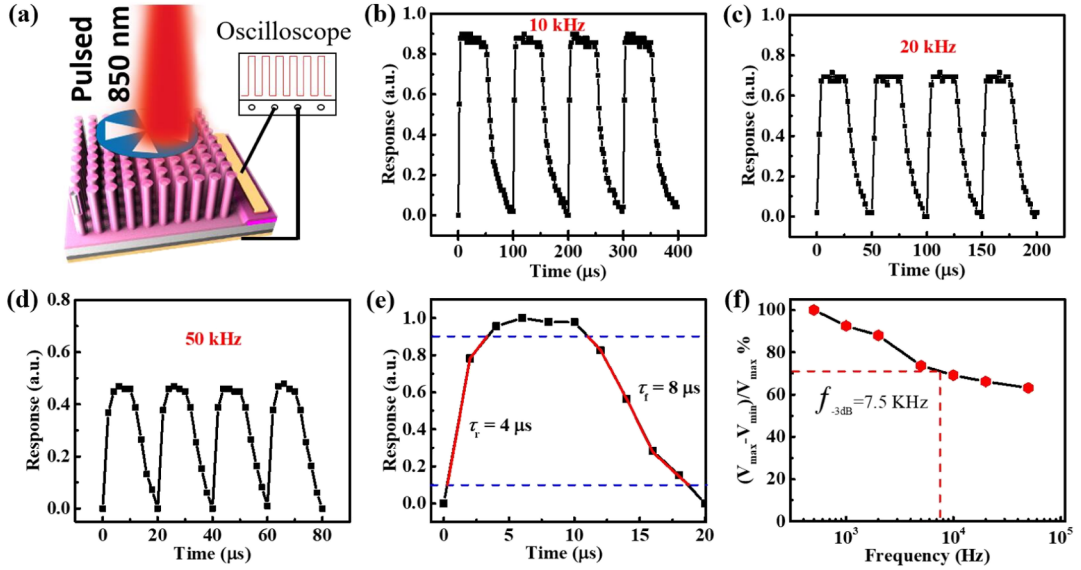

Figure 4. (a) Setup for measuring the photoresponse speed. Photoresponse of the photodiode under fast switching of NIR light with a frequency of (b) 10, (c) 20, and (d) 50 kHz. (e) Individual enlarged cycle for calculating the response speed. (f) Relative balance vs optical frequency.

recombination loss exists in the device and is likely caused by trap states in the heterojunction.[10,11] Apart from the photocurrent, the I_{light}/I_{dark} ratio is also observed to rise monotonously with the increase of NIR intensity. Specifically, the highest ratio is around 1.2×10^4 under light intensity of 6.68 mW cm^{-2} (Figure 3c).

To quantitatively assess the photosensitivity of the SiNW array/perovskite photodetector, two critical performance parameters, responsivity (R), and specific detectivity (D^*) were computed through the following equations[32]

$$R(\mathrm{AW}^{-1}) = \frac{I_{light} - I_{dark}}{P_{in}S} \quad (1)$$

$$D^* = \frac{A^{1/2}R}{(2qI_{dark})^{1/2}} \quad (2)$$

in which I_{light} denotes the current under illumination, I_{dark} is the dark current, P_{in} is the NIR intensity, S is the illuminated area (0.25 cm^2), A is the device area (equal to S in this work), and q is the elementary charge, respectively. Accordingly, R and D^* of the SiNW/perovskite heterojunction photodetector are estimated to be 14.86 mA W^{-1} and 2.04×10^{10} Jones, respectively, at an NIR intensity of 0.892 μW cm^{-2} at 0 V bias. Figure 3d plots R at different intensities. Clearly, the R value increases with decreasing light intensity, which further confirms the presence of recombination loss in the device. This finding is understandable because the photogenerated charge carriers usually recombine more severely at elevated light intensity.[32]

It should be noted that the photoresponse of our heterostructures photodetector also highly depends on the working bias voltage. Figure 3e depicts the time-dependent photoresponse of the photodiode obtained at varied reverse voltages. Remarkably, the photocurrent is significantly enhanced from ~6.7 to ~98.5 μA, when increasing the operational bias from −0.1 to −0.9 V. However, further analysis finds that the I_{light}/I_{dark} ratio decreases remarkably by at least 2 orders of magnitude because of the greatly increased dark current at reverse bias, in comparison with the result at zero bias. Even so, the net photocurrent still increases with the increase of reverse bias. As a matter of fact, this finding is reasonable in that large electric field with the same direction is beneficial for separation and drift of photoinduced electron−hole pairs and therefore suppression of recombination. Additionally, at reverse bias, the depletion region can be extended at heterojunction interface, which allows more photogenerated carriers to take part in the formation of photocurrent. Furthermore, we calculated the R and D^* values of the device at different working biases. As shown in Figure 3f, similar to the photocurrent, both R and D^* rise with increasing operational bias as well, reaching maximum values of 844.33 mA/W and 3.2×10^{11} Jones, respectively, at the bias of −0.9 V. Significantly, as summarized in Table 1, the responsivity and specific detectivity are close to or even better than some SiNW array photodetectors with similar architectures[19,21,22] and

DOI: 10.1021/acsami.8b08387
ACS Appl. Mater. Interfaces 2018, 10, 27850−27857

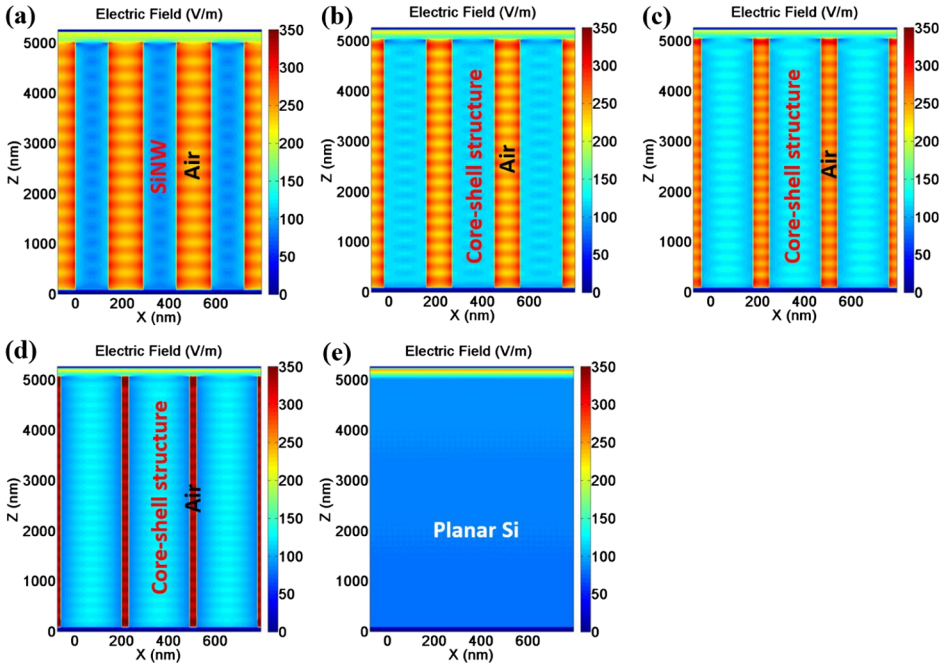

Figure 5. Simulation of electric field density distribution of SiNW array/perovskite core−shell heterostructure with different perovskite thicknesses of (a) 0, (b) 20, (c) 40, (d) 60 nm, and (e) that of planar Si/perovskite (60) nm heterojunction, under 850 nm NIR irradiation, respectively.

perovskite-based heterojunction photodetectors in previous reports.[33−35] The relatively good device performance is due not only to the high quality of SiNWs obtained from chemical etching process but also to the Cs-doped $FAPbI_3$ shell which also displays good electrical property with relatively few defects.

To further explore the feasibility of our heterojunction photodetector for high-frequency optical sensing applications, the photoresponse speed of the photodiode was studied by using an NIR laser diode powered by a function generator and a digital oscilloscope to record the transient photoresponse signal (photovoltage with time). Figure 4a illustrates the schematic setup for response speed measurement. As depicted in Figure 4b−d, the present device can be easily switched between on and off modes for all measured frequencies of 10, 20, and 50 kHz, with excellent reproducibility. Note that even at the frequency as high as 50 kHz, although the photoresponse suffers from somewhat degradation, the photodiode can also probe the rapidly varying photonic pulse. From a single enlarged photoresponse cycle shown in Figure 4e, the rise/fall time (τ_r/τ_f is the duration needed for the photocurrent to increase/decrease from 0.1/0.9 to 0.9/0.1, respectively) are estimated to be 4/8 μs, respectively. It is worth noting that such a speed is faster than other reported SiNW array photodetectors with similar architectures and perovskite-based heterojunction photodetectors (see Table 1) and is nearly close to that of commercial silicon photodiodes.[36] Figure 4f plots the relative balance $(V_{max} - V_{min})/V_{max}$ at different switching frequencies. It is observed that the NIR photodiode shows a slow decay of the relative balance, and it only decreases by around 40% even the frequency is as high as 50 kHz. Furthermore, the 3 dB bandwidth (e.g., the frequency for the photocurrent to reduce to the 70.7% of its peak value) is deduced to be ~7.5 kHz. These findings suggest that the SiNW array/Cs-doped $FAPbI_3$ heterostructure photodiode can operate properly in a wide switching frequency region, which is of pivotal importance for monitoring ultrafast optical signals.

To shed light on the influence of core−shell geometry on the optical property and thus the photoresponse of the heterojunction device, the electric-field density distributions of SiNW array/perovskite core−shell heterostructure with varied perovskite shell layer thicknesses of 0, 20, 40, and 60 nm and planar Si/perovskite (60 nm) heterostructure were compared via numerical calculation based on FEM. To simplify the model, the diameter of the NW and the space between adjacent NWs are set to be 140 and 150 nm, respectively. As observed in Figure 5a, hot spots with strong electric field can be found at superficial region of the SiNWs when illuminated by 850 nm light, suggesting that incident NIR light could be easily confined into the NW array. Significantly, such a light confinement effect can be further enhanced by coating a perovskite layer onto the SiNW surface. It is obvious that the electric-field intensity at superficial region of the core−shell nanostructure is strengthened when increasing the perovskite layer thickness, and a very high electric field intensity appears with the shell thickness reaching 60 nm (Figure 5b−d). The results indicate that light coupling and trapping are more efficient in SiNW array/perovskite core−shell heterostructure with thicker shell layer. This is understandable because light-trapping effect in vertical NW array usually arises from multiple total internal reflections from the periphery of NWs,[37] and the core−shell nanostructure with a thicker shell layer has narrower space between adjacent nanostructures and larger superficial area of individual nanostructure, which are beneficial for improving the light-trapping effect. It is also worth noting that the excellent optical property of the above NW array structures are in sharp contrast to the structure of planar silicon/perovskite heterostructure, where weak-field penetration depth are observed, indicating very limited light coupling capability (Figure 5e). As a matter of fact, the theoretical simulation results coincide well with the device photoresponse performance. Figure S6 exhibits the $I-V$ curves of SiNW array/perovskite core−shell heterostructures with different perovskite shell-layer thicknesses, together with that

DOI: 10.1021/acsami.8b08387
ACS Appl. Mater. Interfaces 2018, 10, 27850−27857

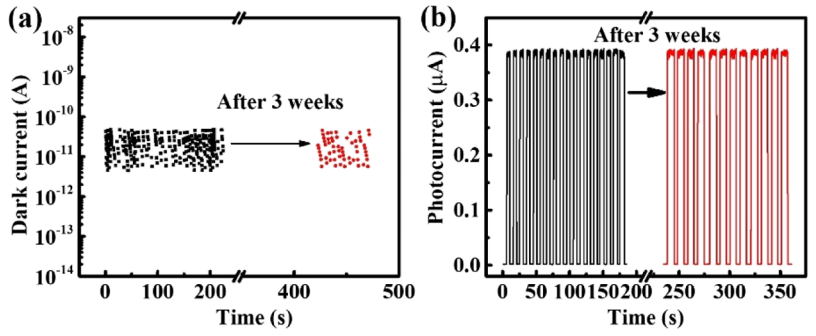

Figure 6. Comparison of (a) dark current and (b) photoresponse of SiNW array/perovskite heterojunction photodetector before and after storage in air for 3 weeks.

of a planar Si/perovskite heterojunction under the same illumination condition. Remarkably, both V_{OC} and I_{SC} values rise with increasing perovskite layer thickness, and the stronger photovoltaic behavior is likely because of the improved light absorption of the core−shell heterojunction with a thicker shell layer. In addition, the planar Si/perovskite heterojunction exhibits the poorest photovoltaic characteristic, which is probably related to its weak optical absorption. On the basis of the above analysis, SiNW array/perovskite core−shell heterojunction with a thicker shell layer is a better choice for realizing high-performance photodetectors.

The long-term air durability of a photodiode is essential for its practical applications. Therefore, the stability of the present SiNW array/Cs-doped $FAPbI_3$ heterostructure photodiode was examined by exposing the device in ambient condition for 3 weeks without any protection. Obviously, the photodiode can still exhibit reversible photoswitching characteristics, with both the dark current and the photocurrent remained almost unchanged after storage, signifying excellent ambient stability (Figure 6a,b). Such good device stability is not only attributed directly to the Cs-doped $FAPbI_3$ perovskite which is more stable than traditional methylammonium lead halide perovskite materials[28] but also probably to the relatively thick perovskite shell layer that can protect the SiNWs from being oxidized in air and thus keep the high quality of the heterojunction interface.[38]

CONCLUSIONS

In summary, a sensitive NIR photodiode was presented by depositing a perovskite thin film onto SiNW array to form a heterojunction with typical core−shell geometry. The strong photovoltaic effect provides the heterojunction with the capability to detect light illumination without voltage supply. The photodetector exhibits good photosensitivity to 850 nm light with a I_{light}/I_{dark} ratio of 1.23×10^4, a responsivity of 14.86 mA/W, a specific detectivity of 2.04×10^{10} Jones, and a photoresponse rate of 4/8 μs, respectively, at 0 V bias. Moreover, both responsivity and specific detectivity values could be increased to be as high as 844.33 mA/W and 3.20×10^{11} Jones, respectively, by applying a working bias of −0.9 V. Further theoretical simulation reveals that the unique core−shell geometry affords excellent optical properties and therefore gives rise to the good device performance.

ASSOCIATED CONTENT

Supporting Information

The Supporting Information is available free of charge on the ACS Publications website at DOI: 10.1021/acsami.8b08387.

SEM image and the corresponding elemental mapping of SiNW/perovskite core−shell nanostructure; XRD pattern of the Cs-doped $FAPbI_3$ perovskite film; $I-V$ curves of Au/perovskite/Au and Ni/p-Si/Ni structures; and $I-V$ curves of different samples under identical illumination condition (850 nm, intensity: 8.87 mW cm^{-2}) (PDF)

AUTHOR INFORMATION

Corresponding Authors

*E-mail: chao.xie@hfut.edu.cn (C.X.).
*E-mail: luolb@hfut.edu.cn (L.-B.L.).
*E-mail: ycwu@hfut.edu.cn (Y.-C.W.).

ORCID

Chao Xie: 0000-0003-4451-767X
Lin-Bao Luo: 0000-0001-8651-8764
Yu-Cheng Wu: 0000-0002-1549-0546

Notes

The authors declare no competing financial interest.

ACKNOWLEDGMENTS

This work was supported by the National Natural Science Foundation of China (NSFC, nos. 51402078, 61675062, and 51672065), the Fundamental Research Funds for the Central Universities (PA2017GDQT0023, JZ2018HGPB0275, and JZ2018HGTA0220), and the China Postdoctoral Science Foundation (103471013).

REFERENCES

(1) Downs, C.; Vandervelde, T. Progress in Infrared Photodetectors Since 2000. *Sensors* **2013**, *13*, 5054−5098.
(2) Martyniuk, P.; Rogalski, A. Quantum-Dot Infrared Photodetectors: Status and Outlook. *Prog. Quantum Electron.* **2008**, *32*, 89−120.
(3) Liang, F.-X.; Wang, J.-Z.; Li, Z.-P.; Luo, L.-B. Near-Infrared-Light Photodetectors Based on One-Dimensional Inorganic Semiconductor Nanostructures. *Adv. Opt. Mater.* **2017**, *5*, 1700081.
(4) Buscema, M.; Island, J. O.; Groenendijk, D. J.; Blanter, S. I.; Steele, G. A.; van der Zant, H. S. J.; Castellanos-Gomez, A. Photocurrent Generation with Two-Dimensional van Der Waals Semiconductors. *Chem. Soc. Rev.* **2015**, *44*, 3691−3718.
(5) Xie, C.; Yan, F. Flexible Photodetectors Based on Novel Functional Materials. *Small* **2017**, *13*, 1701822.
(6) Sze, S. M.; Ng, K. K. *Physics of Semiconductor Devices*; Wiley, 2006.
(7) Tian, W.; Wang, Y.; Chen, L.; Li, L. Self-Powered Nanoscale Photodetectors. *Small* **2017**, *13*, 1701848.

(8) Wang, Y.; Ding, K.; Sun, B.; Lee, S.-T.; Jie, J. Two-Dimensional Layered Material/silicon Heterojunctions for Energy and Optoelectronic Applications. *Nano Res.* **2016**, *9*, 72−93.
(9) Solt, K.; Melchior, H.; Kroth, U.; Kuschnerus, P.; Persch, V.; Rabus, H.; Richter, M.; Ulm, G. PtSi-n-Si Schottky-barrier photodetectors with stable spectral responsivity in the 120-250 nm spectral range. *Appl. Phys. Lett.* **1996**, *69*, 3662−3664.
(10) Li, X.; Zhu, M.; Du, M.; Lv, Z.; Zhang, L.; Li, Y.; Yang, Y.; Yang, T.; Li, X.; Wang, K.; Zhu, H.; Fang, Y. High Detectivity Graphene-Silicon Heterojunction Photodetector. *Small* **2016**, *12*, 595−601.
(11) Wang, L.; Jie, J.; Shao, Z.; Zhang, Q.; Zhang, X.; Wang, Y.; Sun, Z.; Lee, S.-T. MoS2/Si Heterojunction with Vertically Standing Layered Structure for Ultrafast, High-Detectivity, Self-Driven Visible-Near Infrared Photodetectors. *Adv. Funct. Mater.* **2015**, *25*, 2910−2919.
(12) Xie, C.; Wang, Y.; Zhang, Z.-X.; Wang, D.; Luo, L.-B. Graphene/Semiconductor Hybrid Heterostructures for Optoelectronic Device Applications. *Nano Today* **2018**, *19*, 41−83.
(13) An, X.; Liu, F.; Jung, Y. J.; Kar, S. Tunable Graphene-Silicon Heterojunctions for Ultrasensitive Photodetection. *Nano Lett.* **2013**, *13*, 909−916.
(14) Peng, K.-Q.; Lee, S.-T. Silicon Nanowires for Photovoltaic Solar Energy Conversion. *Adv. Mater.* **2011**, *23*, 198−215.
(15) Wang, Y.; Wang, T.; Da, P.; Xu, M.; Wu, H.; Zheng, G. Silicon Nanowires for Biosensing, Energy Storage, and Conversion. *Adv. Mater.* **2013**, *25*, 5177−5195.
(16) Garnett, E.; Yang, P. Light Trapping in Silicon Nanowire Solar Cells. *Nano Lett.* **2010**, *10*, 1082−1087.
(17) Zhang, X.; Xie, C.; Jie, J.; Zhang, X.; Wu, Y.; Zhang, W. High-Efficiency graphene/Si Nanoarray Schottky Junction Solar Cells via Surface Modification and Graphene Doping. *J. Mater. Chem. A* **2013**, *1*, 6593.
(18) Luo, L.-B.; Zeng, L.-H.; Xie, C.; Yu, Y.-Q.; Liang, F.-X.; Wu, C.-Y.; Wang, L.; Hu, J.-G. Light Trapping and Surface Plasmon Enhanced High-Performance NIR Photodetector. *Sci. Rep.* **2015**, *4*, 3914.
(19) Hong, Q.; Cao, Y.; Xu, J.; Lu, H.; He, J.; Sun, J.-L. Self-Powered Ultrafast Broadband Photodetector Based on p-n Heterojunctions of CuO/Si Nanowire Array. *ACS Appl. Mater. Interfaces* **2014**, *6*, 20887−20894.
(20) Manna, S.; Das, S.; Mondal, S. P.; Singha, R.; Ray, S. K. High Efficiency Si/CdS Radial Nanowire Heterojunction Photodetectors Using Etched Si Nanowire Templates. *J. Phys. Chem. C* **2012**, *116*, 7126−7133.
(21) Cao, Y.; Zhu, J.; Xu, J.; He, J.; Sun, J.-L.; Wang, Y.; Zhao, Z. Ultra-Broadband Photodetector for the Visible to Terahertz Range by Self-Assembling Reduced Graphene Oxide-Silicon Nanowire Array Heterojunctions. *Small* **2014**, *10*, 2345−2351.
(22) Xie, C.; Nie, B.; Zeng, L.; Liang, F.-X.; Wang, M.-Z.; Luo, L.; Feng, M.; Yu, Y.; Wu, C.-Y.; Wu, Y.; Yu, S.-H. Core-Shell Heterojunction of Silicon Nanowire Arrays and Carbon Quantum Dots for Photovoltaic Devices and Self-Driven Photodetectors. *ACS Nano* **2014**, *8*, 4015−4022.
(23) Wang, H.; Kim, D. H. Perovskite-Based Photodetectors: Materials and Devices. *Chem. Soc. Rev.* **2017**, *46*, 5204−5236.
(24) Ahmadi, M.; Wu, T.; Hu, B. A Review on Organic-Inorganic Halide Perovskite Photodetectors: Device Engineering and Fundamental Physics. *Adv. Mater.* **2017**, *29*, 1605242.
(25) Tian, W.; Zhou, H.; Li, L. Hybrid Organic-Inorganic Perovskite Photodetectors. *Small* **2017**, *13*, 1702107.
(26) Zhou, J.; Huang, J. Photodetectors Based on Organic-Inorganic Hybrid Lead Halide Perovskites. *Adv. Sci.* **2018**, *5*, 1700256.
(27) Zhang, M.-L.; Peng, K.-Q.; Fan, X.; Jie, J.-S.; Zhang, R.-Q.; Lee, S.-T.; Wong, N.-B. Preparation of Large-Area Uniform Silicon Nanowires Arrays through Metal-Assisted Chemical Etching. *J. Phys. Chem. C* **2008**, *112*, 4444−4450.
(28) Liang, F.-X.; Wang, J.-Z.; Zhang, Z.-X.; Wang, Y.-Y.; Gao, Y.; Luo, L.-B. Broadband, Ultrafast, Self-Driven Photodetector Based on Cs-Doped FAPbI3 Perovskite Thin Film. *Adv. Opt. Mater.* **2017**, *5*, 1700654.
(29) Xia, X.; Wu, W.; Li, H.; Zheng, B.; Xue, Y.; Xu, J.; Zhang, D.; Gao, C.; Liu, X. Spray reaction prepared FA1−xCsxPbI3 solid solution as a light harvester for perovskite solar cells with improved humidity stability. *RSC Adv.* **2016**, *6*, 14792−14798.
(30) Chen, Q.; De Marco, N.; Yang, Y.; Song, T.-B.; Chen, C.-C.; Zhao, H.; Hong, Z.; Zhou, H.; Yang, Y. Under the Spotlight: The Organic-Inorganic Hybrid Halide Perovskite for Optoelectronic Applications. *Nano Today* **2015**, *10*, 355−396.
(31) Zhao, Y.; Zhu, K. Organic-inorganic hybrid lead halide perovskites for optoelectronic and electronic applications. *Chem. Soc. Rev.* **2016**, *45*, 655−689.
(32) Xie, C.; Mak, C.; Tao, X.; Yan, F. Photodetectors Based on Two-Dimensional Layered Materials Beyond Graphene. *Adv. Funct. Mater.* **2017**, *27*, 1603886.
(33) Zhou, H.; Song, Z.; Tao, P.; Lei, H.; Gui, P.; Mei, J.; Wang, H.; Fang, G. Self-powered, ultraviolet-visible perovskite photodetector based on TiO2 nanorods. *RSC Adv.* **2016**, *6*, 6205−6208.
(34) Wang, Z.; Yu, R.; Pan, C.; Li, Z.; Yang, J.; Yi, F.; Wang, Z. L. Light-Induced Pyroelectric Effect as an Effective Approach for Ultrafast Ultraviolet Nanosensing. *Nat. Commun.* **2015**, *6*, 8401.
(35) Alwadai, N.; Haque, M. A.; Mitra, S.; Flemban, T.; Pak, Y.; Wu, T.; Roqan, I. High-Performance Ultraviolet-to-Infrared Broadband Perovskite Photodetectors Achieved via Inter-/Intraband Transitions. *ACS Appl. Mater. Interfaces* **2017**, *9*, 37832−37838.
(36) Bae, J.; Kim, H.; Zhang, X.-M.; Dang, C. H.; Zhang, Y.; Choi, Y. J.; Nurmikko, A.; Wang, Z. L. Si nanowire metal-insulator-semiconductor photodetectors as efficient light harvesters. *Nanotechnology* **2010**, *21*, 095502.
(37) Cao, L.; Fan, P.; Vasudev, A. P.; White, J. S.; Yu, Z.; Cai, W.; Schuller, J. A.; Fan, S.; Brongersma, M. L. Semiconductor Nanowire Optical Antenna Solar Absorbers. *Nano Lett.* **2010**, *10*, 439−445.
(38) Song, Y.; Li, X.; Mackin, C.; Zhang, X.; Fang, W.; Palacios, T.; Zhu, H.; Kong, J. Role of Interfacial Oxide in High-Efficiency Graphene-Silicon Schottky Barrier Solar Cells. *Nano Lett.* **2015**, *15*, 2104−2110.

DOI: 10.1021/acsami.8b08387
ACS Appl. Mater. Interfaces 2018, 10, 27850−27857